New Journal of Physics
The open–access journal for physics

Relativistic formulation of the Korringa–Kohn–Rostoker nonlocal coherent-potential approximation

D Ködderitzsch[1], H Ebert[1], D A Rowlands[2] and A Ernst[3]

[1] Ludwig-Maximilians-Universität München, Department Chemie und Biochemie, Physikalische Chemie, Butenandtstraße 11, D-81377 München, Germany
[2] H H Wills Physics Laboratory, University of Bristol, Bristol BS8 1TL, UK
[3] Max-Planck-Institut für Mikrostrukturphysik, Weinberg 2, D-06120 Halle, Germany
E-mail: diemo.koedderitzsch@cup.uni-muenchen.de

New Journal of Physics **9** (2007) 81
Received 16 November 2006
Published 3 April 2007
Online at http://www.njp.org/
doi:10.1088/1367-2630/9/4/081

Abstract. The recently introduced Korringa–Kohn–Rostoker nonlocal coherent-potential approximation (KKR-NLCPA) provides a sound basis for systematically including important environmental effects within an *ab initio* description of disordered systems. Here we propose a fully relativistic formulation of the KKR-NLCPA which is designed for the treatment of magnetically-ordered alloys. Crucial to its implementation is a reformulation of the basic algorithm and a symmetrization of the fundamental coarse-graining procedure, which we describe in detail. As a first application of the approach we study the electronic and magnetic properties of the ferromagnetic FePt system.

PII: S1367-2630(07)37398-9

Contents

1. Introduction

The coherent potential approximation (CPA) [1] is nowadays widely used to calculate the electronic structure of disordered systems. In particular, its implementation within the Korringa–Kohn–Rostoker (KKR) [2, 3] multiple scattering framework can be combined compatibly with density functional theory, and has thus turned out to be a very powerful and flexible technique. Applications have been made so far to a broad class of materials including random alloys showing split-band behaviour such as Cu_xZn_{1-x}, or alloys with very different components as far as exchange splitting and spin–orbit coupling is concerned, e.g. Fe_xPt_{1-x} [4]. Also, a very broad ranged spectrum of physical properties of random alloys have been studied using the KKR-CPA, for example spectroscopic [5] and transport properties [6].

In spite of its wide application, the CPA has a natural limitation because it is a single-site mean-field theory. Using the KKR-multiple scattering formalism the corresponding effective medium that is meant to represent the configurational average of a random alloy of given concentration is constructed by demanding that embedding an A or B atom of an alloy A_xB_{1-x} as an isolated impurity into the medium should not lead on average to additional scattering. This prescription obviously does not allow us to investigate fluctuations around the CPA average nor to account for the influence of atomic short-range order. Accordingly, several schemes have been developed in the past to overcome these limitations by developing a cluster generalization of the CPA. Many of the early attempts to formulate CPA extensions had difficulties in yielding results with the correct analytical (Herglotz) properties. Those proven to be analytic include the molecular CPA [7], the travelling cluster approximation (TCA) [8], the cluster CPA (C-CPA) [9] and the embedded cluster method (ECM) [10] (for an overview see [11], [12]), although there remain shortcomings and problems connected with these techniques [11]. However, these shortcomings can be remedied by the recent introduction of the nonlocal CPA (NLCPA) [13] based on the dynamical cluster approximation (DCA) [14], which has been proved to be analytic. The NLCPA was subsequently derived within the framework of KKR [15, 16].

Similar to the standard CPA, the NLCPA introduces a translationally invariant effective medium. Using the KKR method this medium can be defined by a corresponding NLCPA condition that demands that embedding of atomic clusters should on average lead to no excess scattering. Although the resulting NLCPA scheme is numerically more demanding than the standard CPA scheme, the first implementation [17, 18] has been done recently followed by

others [19]. A fully charge self-consistent version has also been recently implemented [20] based on a total energy formulation which systematically takes into account the effects of charge correlations (the Madelung energy). In contrast to approaches such as the locally self-consistent Green function method [21]–[23] and the polymorphous CPA [24] which are specially designed for the treatment of large systems using supercells that contain hundreds or even thousands of atoms, such self-consistent-field (SCF)-KKR-NLCPA calculations can be done on a single processor machine with reasonable efforts.

In this paper, we discuss the extension of the NLCPA scheme to the relativistic treatment of magnetically-ordered systems. Crucial to its implementation is a robust iteration algorithm together with the extensive use of symmetry. To do the former we show how a reformulation of the original KKR-NLCPA algorithm [16] that avoids the use of the free electron Green's function can be recast into an NLCPA generalization of the so-called Mills-CPA-algorithm [8, 25]. To do the latter we introduce a scheme for reducing the Brillouin zone integration volume to that of the irreducible wedge of the underlying lattice. The flexibility and power of the resulting approach is demonstrated by application to the alloy system $Fe_{0.5}Pt_{0.5}$.

2. Relativistic formulation of the KKR-NLCPA

2.1. The basic equations

Within multiple scattering theory the KKR-NLCPA medium is represented by the corresponding single-site t-matrix $\hat{\underline{t}}$, the scattering path operator $\hat{\underline{\tau}}^{ij}$ and the effective structure constant corrections $\delta\hat{\underline{G}}$ that account for all nonlocal scattering corrections due to disorder configurations (for more details see [16, 18]). Here and in the following the circumflex indicates a quantity connected with the KKR-NLCPA medium. An underscore denotes matrices with respect to a particular representation. Within a non-relativistic formulation the L-representation is used in general with $L = (l, m_l)$ combining the angular momentum and magnetic quantum numbers, l and m_l, respectively. For the relativistic Λ-representation used below, $\Lambda = (\kappa, \mu)$ combines the relativistic spin–orbit and magnetic quantum numbers, κ and μ, respectively [26].

To determine the above mentioned quantities self-consistently a coarse graining procedure is applied. This implies in particular the introduction of a set of N_c real space cluster sites $\{I\}$ together with a corresponding set of cluster momenta $\{\mathbf{K}_n\}$ [18]. This procedure leads to a subdivision of reciprocal space into non-overlapping tiles centred around the vectors $\mathbf{K}_n$, with N_c tiles covering the Brillouin zone volume. Within a tile centred at $\mathbf{K}_n$ the Fourier transform $\delta\hat{\underline{G}}(\mathbf{k})$ of $\delta\hat{\underline{G}}^{ij}$ is approximated by $\delta\hat{\underline{G}}(\mathbf{K}_n)$, being the average of $\delta\hat{\underline{G}}(\mathbf{k})$ over the tile. According to the construction of the real space cluster and its corresponding set $\{\mathbf{K}_n\}$, $\delta\hat{\underline{G}}(\mathbf{K}_n)$ is connected to its counterpart in real space via

$$\delta\hat{\underline{G}}^{IJ} = \frac{1}{N_c}\sum_{\mathbf{K}_n}\delta\hat{\underline{G}}(\mathbf{K}_n)\mathrm{e}^{i\mathbf{K}_n(\mathbf{R}_I-\mathbf{R}_J)}, \tag{1}$$

$$\delta\hat{\underline{G}}(\mathbf{K}_n) = \sum_{I\neq J}\delta\hat{\underline{G}}^{IJ}\mathrm{e}^{-i\mathbf{K}_n(\mathbf{R}_I-\mathbf{R}_J)}, \tag{2}$$

with I and J denoting the cluster sites at $\mathbf{R}_I$ and $\mathbf{R}_J$, respectively (note, that from now on capital indices exclusively enumerate sites within the cluster). In line with the coarse-graining procedure applied to $\delta\hat{\underline{G}}(\mathbf{k})$ one has for the scattering path operator in reciprocal and real space

$$\hat{\underline{\tau}}(\mathbf{K}_n) = \frac{1}{V_{\mathbf{K}_n}} \int_{(V_{\mathbf{K}_n})} \mathrm{d}^3k \, [\hat{\underline{m}} - \delta\hat{\underline{G}}(\mathbf{K}_n) - \underline{G}(\mathbf{k})]^{-1}, \tag{3}$$

$$\hat{\underline{\tau}}^{IJ} = \frac{1}{N_\mathrm{c}} \sum_{\mathbf{K}_n} \hat{\underline{\tau}}(\mathbf{K}_n) \mathrm{e}^{\mathrm{i}\mathbf{K}_n(\mathbf{R}_I - \mathbf{R}_J)}. \tag{4}$$

In equation (3) $V_{\mathbf{K}_n}$ is the volume of the tile centred at $\mathbf{K}_n$ and $\underline{G}(\mathbf{k})$ is the standard KKR structure constants matrix. In addition, $\hat{\underline{m}} = \hat{\underline{t}}^{-1}$ represents the inverse of the KKR-NLCPA single-site t-matrix.

Within the framework sketched above the standard single-site CPA approach can consistently be generalized to a cluster formulation. This leads to the corresponding KKR-NLCPA condition

$$\hat{\underline{\tau}}^{IJ} = \sum_\gamma P_\gamma \underline{\tau}_\gamma^{IJ}, \tag{5}$$

stating that the scattering path operator of the effective KKR-NLCPA medium is identical to the average of the scattering path operators for clusters with configurations γ of N_c atoms embedded into the KKR-NLCPA medium. The set of numbers $\{P_\gamma\}$ contain the weights for the configurations γ with $\sum_\gamma P_\gamma = 1$. Using the degrees of freedom in the choice of the probability distribution $\{P_\gamma\}$, the NLCPA allows us to study short-range order effects. As $\underline{\tau}_\gamma^{IJ}$ depends on the single-site t-matrices of the embedded real atoms ($\underline{t}^\mathrm{A}$ and $\underline{t}^\mathrm{B}$ for a binary alloy $\mathrm{A}_x\mathrm{B}_{1-x}$) as well as on $\hat{\underline{\tau}}^{IJ}$ one is led to a set of equations that has to be solved iteratively for $\hat{\underline{t}}$, $\hat{\underline{\tau}}^{IJ}$ and $\delta\hat{\underline{G}}^{IJ}$.

An extension of the existing non-relativistic NLCPA formalism to a relativistic one is obtained by expressing all the above mentioned quantities in a relativistic (κ, μ)-representation. The Green's function is constructed from the regular $Z_\Lambda^n(\vec{r}, E)$ and irregular solutions $J_\Lambda^n(\vec{r}, E)$ of the single site problem (i.e. the Dirac equation for a given potential) at site n by using the relativistic scattering path operator [27], i.e.

$$\begin{aligned} G(\mathbf{r}, \mathbf{r}', E) = \sum_{\Lambda\Lambda'} Z_\Lambda^n(\mathbf{r}, E) \tau_{\Lambda\Lambda'}^{nn'}(E) Z_{\Lambda'}^{n'\times}(\mathbf{r}', E) - \sum_\Lambda \big[Z_\Lambda^n(\mathbf{r}, E) J_\Lambda^{n\times}(\mathbf{r}', E)\, \Theta(r' - r) \\ + J_\Lambda^n(\mathbf{r}, E) Z_\Lambda^{n\times}(\mathbf{r}', E)\, \Theta(r - r') \big] \delta_{nn'} \end{aligned}$$

The averaging procedure follows the one given in [15, 16] so that

$$\bar{G}(\mathbf{r}, \mathbf{r}', E) = \sum_{\Lambda\Lambda'} \left[\sum_{\gamma\alpha} P(\alpha, \gamma) Z_\Lambda^\alpha(\mathbf{r}_I, E) \langle \tau_{\Lambda\Lambda'}^{II} \rangle_{\alpha,\gamma} Z_{\Lambda'}^{\alpha\times}(\mathbf{r}_I, E) \right] - \sum_{\Lambda\alpha} P(\alpha) Z_\Lambda^\alpha(\mathbf{r}_I, E) J_\Lambda^{\alpha\times}(\mathbf{r}_I, E).$$

Here $P(\alpha, \gamma)$ denotes the probability of a cluster configuration with an α-atom at the site I in a cluster with configuration γ. Using the NLCPA approximation $\langle \tau_{\Lambda\Lambda'}^{II} \rangle_{\alpha,\gamma}$ is constructed from an impurity cluster of configuration (α, γ) embedded in the NLCPA effective medium. The resulting approximation to the average, $\tilde{G}$, is translationally-invariant and does not depend on the choice for the cluster site I. Using $\tilde{G}$ one can access the density of states (DOS),

spin- and orbital-magnetic moments, etc, in the usual way, e.g. the DOS as integral over the volume V_I of site I

$$\bar{n}(E) = -\frac{1}{\pi}\mathrm{ImTrace}\int_{V_I}\tilde{G}(\mathbf{r},\mathbf{r},E)\,\mathrm{d}^3\mathrm{r},$$

or charge, spin- and orbital moments by using the operators $\mathcal{A}=1$, $\mathcal{A}=\beta\hat{\Sigma}_z$ and $\mathcal{A}=\beta\hat{l}_z$, respectively, in the following expression

$$\langle\mathcal{A}\rangle = -\frac{1}{\pi}\mathrm{ImTrace}\int^{E_F}\mathrm{d}E\,\mathcal{A}\tilde{G}(\mathbf{r},\mathbf{r},E).$$

Please note, that in the our approach the spin–orbit coupling is not treated as a perturbation but accounted for by solving the associated single-site equations for Z and J in a fully relativistic way.

2.2. A robust and efficient KKR-NLCPA algorithm

First note that the algorithm suggested in [16] involves the real space cluster structure constants matrix $\underline{\underline{G}}$, where the second underscore indicates a matrix with respect to the cluster sites $\{I\}$. Its inclusion is however purely formal, i.e. to facilitate the scattering within the cluster. In practice it is not actually necessary to involve $\underline{\underline{G}}$ since this matrix can be straightforwardly eliminated in all expressions [15]. This leads to the following modified KKR-NLCPA algorithm.

1. In the first iteration make a guess for the effective cluster t-matrix $\hat{t}^{IJ}_{\mathrm{cl}}$ by putting an effective scatterer $\bar{\underline{t}}$ on every site-diagonal block: $\hat{\underline{\underline{t}}}_{\mathrm{cl}} = \bar{\underline{t}}\otimes\mathbb{I}_{N_\mathrm{c}}$. $\bar{\underline{t}}$ can be approximated by use of the average t-matrix approximation (ATA) [11]: $\bar{\underline{t}} = P(A)\underline{t}^{\mathrm{A}} + P(B)\underline{t}^{\mathrm{B}}$ with $P(\alpha)$ being the probability for the occupation of site I by component α, or starting from a previous CPA calculation: $\bar{\underline{t}} = \underline{t}^{\mathrm{CPA}}$. As mentioned above $\hat{\underline{\underline{m}}}_{\mathrm{cl}} = (\hat{\underline{\underline{t}}}_{\mathrm{cl}})^{-1}$.
2. Combine the site-off diagonal translationally invariant effective disorder term $\delta\hat{\underline{G}}^{IJ}$ and the (site diagonal) inverse of the effective t-matrix $\hat{\underline{\underline{m}}}$

$$\hat{\underline{\underline{\mu}}} \equiv \hat{\underline{\underline{m}}} - \delta\hat{\underline{\underline{G}}} = \hat{\underline{\underline{m}}}_{\mathrm{cl}} + \underline{\underline{G}}.$$

   In the first iteration $\delta\hat{\underline{\underline{G}}}$ is set to zero.
3. Use a Fourier transformation to convert the matrix elements of $\hat{\underline{\underline{\mu}}}$ to coarse-grained reciprocal space

$$\hat{\underline{\mu}}(\mathbf{K}_n) = \frac{1}{N_\mathrm{c}}\sum_{I\neq J}\hat{\underline{\mu}}^{IJ}\mathrm{e}^{-\mathrm{i}\mathbf{K}_n(\mathbf{R}_I-\mathbf{R}_J)}, \tag{6}$$

   where $\hat{\underline{\mu}}(\mathbf{K}_n) = \hat{\underline{m}} - \delta\hat{\underline{G}}(\mathbf{K}_n)$.
4. Calculate the coarse grained matrix elements $\hat{\underline{\tau}}(\mathbf{K}_n)$ with the modified equation (3)

$$\hat{\underline{\tau}}(\mathbf{K}_n) = \frac{1}{V_{\mathbf{K}_n}}\int_{(V_{\mathbf{K}_n})}\mathrm{d}^3k[\hat{\underline{\mu}}(\mathbf{K}_n) - \hat{\underline{G}}(\mathbf{k})]^{-1}, \tag{7}$$

   and use equation (4) to get the real space scattering path operator $\hat{\underline{\tau}}^{IJ} = (\hat{\underline{\tau}})^{IJ}$.

5. Determine the auxiliary quantity $\hat{\underline{\underline{\Omega}}}$ that combines the effective cluster renormalized interactor $\hat{\underline{\underline{\Delta}}}$ and the real space Green's function $\underline{\underline{G}}$

$$\hat{\underline{\underline{\Omega}}} = \hat{\underline{\underline{\Delta}}} + \underline{\underline{G}} = \hat{\underline{\underline{m}}}_{\mathrm{cl}} + \underline{\underline{G}} - \hat{\underline{\underline{\tau}}}^{-1} = \hat{\underline{\underline{\mu}}} - \hat{\underline{\underline{\tau}}}^{-1}.$$

6. Do a loop over the 2^{N_c} cluster configurations. For a particular cluster configuration fill up the cavity and determine

$$\underline{\underline{\tau}}_{\gamma} = [\underline{\underline{m}}_{\gamma} - \hat{\underline{\underline{\Omega}}}]^{-1}.$$

Here $\underline{\underline{m}}_{\gamma}$ is a site diagonal matrix with $\underline{m}_{\gamma}^{II}$ being equal either to $\underline{m}_{\mathrm{A}}$ or $\underline{m}_{\mathrm{B}}$ depending on the configuration γ. Average over the configurations according to equation (5) to obtain a new effective scattering path operator

$$\hat{\underline{\underline{\tau}}} = \sum_{\gamma} P_{\gamma} \underline{\underline{\tau}}_{\gamma}. \tag{8}$$

7. Update the auxiliary matrix $\hat{\underline{\underline{\mu}}}$

$$\hat{\underline{\underline{\mu}}} = \hat{\underline{\underline{m}}}_{\mathrm{cl}} + \underline{\underline{G}} = \hat{\underline{\underline{\tau}}}^{-1} + \hat{\underline{\underline{\Omega}}}. \tag{9}$$

Check for convergence—if not converged proceed with step 3.

By performing the NLCPA iterations using $\hat{\underline{\underline{\mu}}}$, $\hat{\underline{\underline{\tau}}}$ and $\hat{\underline{\underline{\Omega}}}$ instead of $\hat{\underline{\underline{m}}}_{\mathrm{cl}}$, $\hat{\underline{\underline{\tau}}}$, $\hat{\underline{\underline{\Delta}}}$ it is clear that $\underline{\underline{G}}$ is not needed. The inverse of the NLCPA single-site t-matrix is nevertheless available as the following relation holds due to the fact the site-diagonal blocks of $\delta\hat{\underline{\underline{G}}}$ are zero

$$\hat{\underline{\mu}}^{II} = \hat{\underline{m}}_{\mathrm{cl}}^{II} = \hat{\underline{m}}, \quad \forall I.$$

In some cases it helps to apply the simple mixing

$$\hat{\underline{\underline{\mu}}}_{\mathrm{in}}^{(n+1)} = (1-\alpha)\hat{\underline{\underline{\mu}}}_{\mathrm{out}}^{(n)} + \alpha\hat{\underline{\underline{\mu}}}_{\mathrm{in}}^{(n)}, \qquad \alpha \in [0,1],$$

when updating $\hat{\underline{\underline{\mu}}}$ in step 7, where $\hat{\underline{\underline{\mu}}}_{\mathrm{in}}^{(n)}$ enters equation (6), $\hat{\underline{\underline{\mu}}}_{\mathrm{out}}^{(n)}$ is obtained from equation (9) and the mixing parameter α is chosen carefully.

The NLCPA algorithm sketched above will converge well in some situations, however in general, and especially for relativistic calculations, convergence is very slow or cannot be reached at all. The next step in the reformulation of the algorithm is to generalize an idea which goes back to the work of Mills *et al* [8, 25], and recast the NLCPA condition equation (8) into

$$0 = \sum_{\gamma} P_{\gamma}(\underline{\underline{\tau}}_{\gamma} - \hat{\underline{\underline{\tau}}}) = \sum_{\gamma} P_{\gamma}[(\underline{\underline{m}}_{\gamma} - \hat{\underline{\underline{\mu}}} + \hat{\underline{\underline{\tau}}}^{-1})^{-1} - \hat{\underline{\underline{\tau}}}] = -\hat{\underline{\underline{\tau}}}\left[\sum_{\gamma} P_{\gamma}[(\underline{\underline{m}}_{\gamma} - \hat{\underline{\underline{\mu}}})^{-1} + \hat{\underline{\underline{\tau}}}]^{-1}\right]\hat{\underline{\underline{\tau}}}.$$

By demanding that

$$0 = \sum_{\gamma} P_{\gamma}[(\underline{\underline{m}}_{\gamma} - \hat{\underline{\underline{\mu}}})^{-1} + \hat{\underline{\underline{\tau}}}]^{-1} = \sum_{\gamma} P_{\gamma}\underline{\underline{X}}_{\gamma} \tag{10}$$

with

$$\underline{\underline{X}}_\gamma = \left[(\underline{\underline{m}}_\gamma - \underline{\underline{\hat{\mu}}})^{-1} + \underline{\underline{\hat{\tau}}}\right]^{-1},$$

an alternative form for the NLCPA-condition is obtained.[4] The expression on the right-hand side of equation (10) evaluated in the nth iteration can be regarded as a residual error matrix

$$\underline{\underline{E}}^{(n)} = -\sum_\gamma P_\gamma \underline{\underline{X}}_\gamma^{(n)} \longrightarrow 0,$$

which has to go to zero upon convergence. This residual error is a result of working with $\underline{\underline{\hat{\mu}}}^{(n)}$ instead of the converged $\underline{\underline{\hat{\mu}}}^{(\infty)}$. Accordingly, one has

$$-\underline{\underline{E}}^{(n)} = \left[(\underline{\underline{\hat{\mu}}}^{(\infty)} - \underline{\underline{\hat{\mu}}}^{(n)})^{-1} + \underline{\underline{\hat{\tau}}}^{(n)}\right]^{-1},$$

which leads to

$$\underline{\underline{\hat{\mu}}}^{(\infty)} = \underline{\underline{\hat{\mu}}}^{(n)} - \left[(\underline{\underline{E}}^{(n)})^{-1} + \underline{\underline{\hat{\tau}}}^{(n)}\right]^{-1}.$$

Therefore, we use the following guess for the next iteration

$$\underline{\underline{\hat{\mu}}}^{(n+1)} = \underline{\underline{\hat{\mu}}}^{(n)} - \left[(\underline{\underline{E}}^{(n)})^{-1} + \underline{\underline{\hat{\tau}}}^{(n)}\right]^{-1} = \underline{\underline{\hat{\mu}}}^{(n)} - \left[1 + \underline{\underline{E}}^{(n)}\underline{\underline{\hat{\tau}}}^{(n)}\right]^{-1} \underline{\underline{E}}^{(n)}.$$

The last step avoids working with the inverse of the error matrix which will become singular upon convergence. This modified Mills-algorithm can also further be stabilized by averaging and symmetrizing the site diagonal blocks of $\underline{\underline{\hat{\mu}}}$ and $\underline{\underline{\hat{\tau}}}$ over the sites I of the cluster. This procedure is based on the observation that the site-diagonal blocks of the former matrices have to be identical because of the translational symmetry of the NLCPA medium (this is also reflected by equation (4) that shows that $\underline{\underline{\hat{\tau}}}^{II}$ is independent of the site index I)

$$\underline{\underline{\hat{\mu}}}^{II}_{\text{avg}} = \frac{1}{N_\text{c}} \sum_J \underline{\underline{\hat{\mu}}}^{JJ}.$$

An additional means to stabilize the NLCPA algorithm is to symmetrize $\underline{\underline{\hat{\mu}}}^{II}$ and $\underline{\underline{\hat{\tau}}}^{II}$ according to the symmetry of the system at hand. For a system with one atom per unit cell treated in a non-relativistic way one has, for example

$$\underline{\underline{\hat{\mu}}}^{II}_{\text{sym}} = \frac{1}{N_U} \sum_U \underline{\underline{U}}\,\underline{\underline{\hat{\mu}}}^{JJ}\,\underline{\underline{U}}^{-1},$$

for N_U symmetry operations U (see below). Corresponding stabilizing procedures could be applied to the site-off diagonal blocks as well but do not seem to be necessary in general.

Using the above method leads to a very satisfactory convergence behaviour for a broad class of systems. Using the maximum norm on the difference $\underline{\underline{\hat{\mu}}}^{(n-1)} - \underline{\underline{\hat{\mu}}}^{(n)}$ for measuring the error in

[4] Here, we ignore the possibility that the product $\underline{\underline{A}}\,\underline{\underline{B}}$ can be zero even for neither $\underline{\underline{A}}$ nor $\underline{\underline{B}}$ being zero.

the nth iteration we typically obtain a decrease in error of one order of magnitude per iteration. Mills *et al* [8] showed that the Mills-algorithm is guaranteed to converge if the ATA is used as a starting guess (see step 1 at the beginning of section 2.2). As the structure of the equations is the same for the CPA and the NLCPA this should also apply here without modifications. In practice, however, it turned out that starting the NLCPA iteration using a converged CPA-result as a starting guess is more efficient.

2.3. Coarse-graining and symmetry

Within standard band structure calculations, symmetry considerations allow us to restrict Brillouin zone integrations to an irreducible wedge. This also applies when calculating the scattering path operator within the standard CPA [28]. Instead of dealing with the volume V_{BZ} of the first Brillouin zone one can restrict the integration to a volume $V_{\mathrm{IBZ}} = V_{\mathrm{BZ}}/h_{\mathcal{G}}$, where $h_{\mathcal{G}}$ is the order of the crystallographic point group $\mathcal{G}$ [29]. To make the KKR-NLCPA a computationally tractable first-principles cluster theory, similar symmetry considerations are introduced here. For example, the Brillouin zone integration (equation (3)) does not scale with the cluster size, and furthermore can be reduced to involve the irreducible wedge corresponding to the symmetry of the effective medium. The only computational cost of a KKR-NLCPA calculation over the conventional KKR-CPA is in principle connected with the configurational averaging (equation (5)) in real space. However, all previous KKR-NLCPA implementations have used the full Brillouin zone. Here we detail how to reduce the integration to the irreducible wedge, which is particularly crucial for a relativistic implementation due to the larger matrices involved.

Starting from equations (3) and (4) it seems that because of the presence of $\delta\underline{\hat{G}}(\mathbf{K}_n)$ the integration in equation (3) has to be done for each of the N_c tiles as it was done in all previous implementations of the NLCPA. Nevertheless, one can exploit symmetry to obtain a substantial reduction of the numerical effort when dealing with these equations. In the following it is shown how the set of coarse-graining tiles can be reduced to a set of a few generating tiles. In addition it is explained how the volume of a generating tile is reduced to its irreducible size. As shown below it is then possible to restrict the integration also to the volume V_{IBZ} as in the standard CPA. For the sake of clarity we restrict the following derivation to a system with one atom per unit cell. In case of a magnetic system a non-relativistic description is assumed (the relativistic case will be examined later). All other more complex situations can be treated in an analogous way (for the necessary group theoretical extensions see for example [28]).

Starting from the abbreviation

$$\underline{\hat{\tau}}_{\mathbf{K}_n}(\mathbf{k}) = [\underline{\hat{m}} - \delta\underline{\hat{G}}(\mathbf{K}_n) - \underline{G}(\mathbf{k})]^{-1}, \tag{11}$$

we rewrite equation (7) as

$$\underline{\hat{\tau}}(\mathbf{K}_n) = \frac{1}{V_{\mathbf{K}_n}} \int_{(V_{\mathbf{K}_n})} \mathrm{d}^3k \, \underline{\hat{\tau}}_{\mathbf{K}_n}(\mathbf{k}).$$

When dealing with equation (11) one notes that $\delta\underline{\hat{G}}(\mathbf{K}_n)$ has the symmetry of the reciprocal lattice, i.e.

$$\delta\underline{\hat{G}}(U\mathbf{K}_n) = \underline{U}\delta\underline{\hat{G}}(\mathbf{K}_n)\underline{U}^{-1}, \tag{12}$$

where U is a symmetry operation of the system [28] and $\underline{U}$ denotes the corresponding transformation matrix in the L- or Λ-representation, respectively. This relation is a direct consequence of the connection of $\delta\hat{\underline{\underline{G}}}$ and $\underline{\underline{\tau}}$ in real space [16] that ensures that both quantities have the symmetry of the effective NLCPA medium. As can be shown, the definition of $\delta\hat{\underline{G}}(\mathbf{K}_n)$ via equation (2) then directly leads to equation (12). Also, $\delta\hat{\underline{G}}(\mathbf{K}_n)$ has the translational symmetry of reciprocal space

$$\delta\hat{\underline{G}}(\mathbf{K}_n) = \underline{\delta\hat{G}}(\mathbf{K}_n + \mathbf{g}), \tag{13}$$

where $\mathbf{g}$ is a reciprocal lattice vector. The relations in equations (12) and (13) can now be exploited in a twofold way.

2.3.1. Reduction to a set of generating tiles. Using the above definitions one has

$$\begin{aligned}\underline{\hat{\tau}}_{U\mathbf{K}_n}(U\mathbf{k}) &= [\underline{\hat{m}} - \delta\underline{\hat{G}}(U\mathbf{K}_n) - \underline{G}(U\mathbf{k})]^{-1} = [\underline{U}[\underline{U}^{-1}\underline{\hat{m}}\,\underline{U} - \delta\underline{\hat{G}}(\mathbf{K}_n) - \underline{G}(\mathbf{k})]\underline{U}^{-1}]^{-1} \\ &= \underline{U}[\underline{\hat{m}} - \delta\underline{\hat{G}}(\mathbf{K}_n) - \underline{G}(\mathbf{k})]^{-1}\underline{U}^{-1} = \underline{U}\,\underline{\hat{\tau}}_{\mathbf{K}_n}(\mathbf{k})\underline{U}^{-1}.\end{aligned} \tag{14}$$

Therefore, if there is a symmetry operation U that transforms $\mathbf{K}_n$ into $\mathbf{K}'_n = U\mathbf{K}_n$ and the tile around $\mathbf{K}_n$ to that around $\mathbf{K}'_n$ then $\underline{\hat{\tau}}(\mathbf{K}'_n)$ can be generated by $\underline{U}$ using $\underline{\hat{\tau}}(\mathbf{K}_n)$

$$\underline{\hat{\tau}}(\mathbf{K}'_n) = \underline{\hat{\tau}}(U\mathbf{K}_n) = \underline{U}\,\underline{\hat{\tau}}(\mathbf{K}_n)\underline{U}^{-1}. \tag{15}$$

Use of this relation in general leads to a substantial reduction of the number of tiles to be treated. To find out which tiles may be connected by symmetry according to equation (15) it is most convenient to make use of the translational symmetry expressed by equation (13). This allows all tiles to be shifted by a suitable reciprocal lattice vector to have a set of tiles for which the modulus of $\mathbf{K}_n$ with respect to reciprocal lattice vectors is minimal. This is demonstrated in figure 1 for the tiles given in [16] for a body-centred cubic (bcc) lattice and $N_c = 16$. Obviously, a symmetry operation U may only connect two tiles centred at $\mathbf{K}_n$ and $\mathbf{K}'_n$ if these have the same distance from the Γ-point, i.e. if $|\mathbf{K}_n| = |\mathbf{K}'_n|$. For a system with one atom per unit cell the set of tiles splits accordingly into N_s sets of tiles with each set having N_s^m members that have the same $|\mathbf{K}_n|$ and which are connected by a symmetry operation U (if the symmetry of the system is lower than that of the underlying Bravais lattice these sets characterized by the same $|\mathbf{K}_n|$ may split into subsets that are not symmetry related, see below). Again this is demonstrated in figure 1 for a bcc-lattice and $N_c = 16$. In this case we end up with $N_s = 5$ sets having $N_s^m = 1, 6, 6, 2, 1$ members (ordered with increasing $\mathbf{K}_n$, see figure 1). Obviously, one has $N_c = \sum_s N_s^m$. The numbers that may occur for the individual N_s^m are restricted by symmetry, as shown below.

2.3.2. Reduction of the set of $\mathbf{k}$*-points of a generating tile to a set of irreducible ones.* Another consequence of the symmetry properties of $\delta\hat{\underline{G}}(\mathbf{K}_n)$ is expressed in the following relationship

$$\underline{\hat{\tau}}_{UU^{-1}\mathbf{K}_n}(U\mathbf{k}) = \underline{\hat{\tau}}_{\mathbf{K}_n}(U\mathbf{k}) = \underline{U}\,\underline{\hat{\tau}}_{U^{-1}\mathbf{K}_n}(\mathbf{k})\underline{U}^{-1},$$

which is obtained by using equation (14). For $U^{-1}\mathbf{K}_n = \mathbf{K}_n$ one therefore has

$$\underline{\hat{\tau}}_{\mathbf{K}_n}(U\mathbf{k}) = \underline{U}\,\underline{\hat{\tau}}_{\mathbf{K}_n}(\mathbf{k})\underline{U}^{-1}.$$

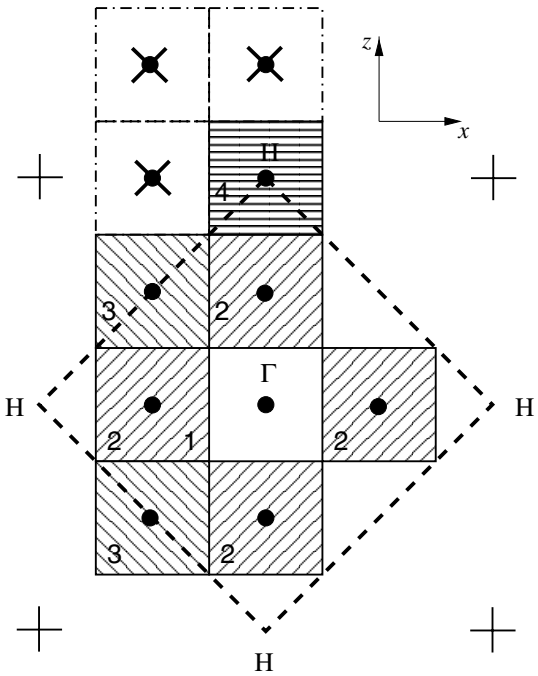

Figure 1. Reordering of the tiles centred at the $\mathbf{K}_n$ given in [16] for a bcc-lattice and $N_c = 16$. Only those tiles with $(\mathbf{K}_n)_y = 0$, i.e. lying in the x–z plane are shown here. The tiles shifted by a reciprocal lattice vector are indicated by a cross (top left part). The various sets of tiles with same $|\mathbf{K}_n|$ are indicated by a common shading and a number. The conventional Brillouin zone is shown with a dashed line and high symmetry points (Γ and H) are indicated. Thin crosses denote reciprocal lattice points.

Here it is important to note that we can exploit the translational symmetry again. Accordingly we accept all point symmetry operations U for which one has

$$\mathbf{K}_n = U\mathbf{K}_n + \mathbf{g}. \tag{16}$$

Therefore, we can replace the integration over the tile by an integration over its irreducible part.

$$\underline{\hat{\tau}}(\mathbf{K}_n) = \sum_U \underline{U} \left[\frac{1}{\tilde{V}_{\mathbf{K}_n}} \int_{(\tilde{V}_{\mathbf{K}_n})} \mathrm{d}^3k [\underline{\hat{\mu}}(\mathbf{K}_n) - \underline{\hat{G}}(\mathbf{k})]^{-1} \right] \underline{U}^{-1}, \tag{17}$$

where $\tilde{V}_{\mathbf{K}_n} = V_{\mathbf{K}_n}/h_{\mathbf{K}_n}$ and $h_{\mathbf{K}_n}$ is the number of symmetry operations U occurring for the tile centred at $\mathbf{K}_n$. The integration over the irreducible volume $\tilde{V}_{\mathbf{K}_n}$ can be done using any standard integration technique. However, it seems that the use of a point sampling technique with a regular grid is most convenient.

The symmetry operations U occurring in equation (17) are restricted according to equation (16) to those that map a $\mathbf{k}$-point within the $\mathbf{K}_n$-centred tile to $\mathbf{k}'$ that lies—apart from a possible shift by a reciprocal lattice vector $\mathbf{g}$—into the same tile. Accordingly, the set of all operations U form a point group $\mathcal{G}_{\mathbf{K}_n}$ of order $h_{\mathbf{K}_n}$. As this point group is at the same time a subset of the crystallographic point group $\mathcal{G}$, $h_{\mathbf{K}_n}$ can take only a limited number of values. For cubic symmetry with $h_{\mathcal{G}} = 48$ one may have $h_{\mathbf{K}_n} = 1, 2, 3, 4, 6, 12, 16, 24$ or 48, respectively.

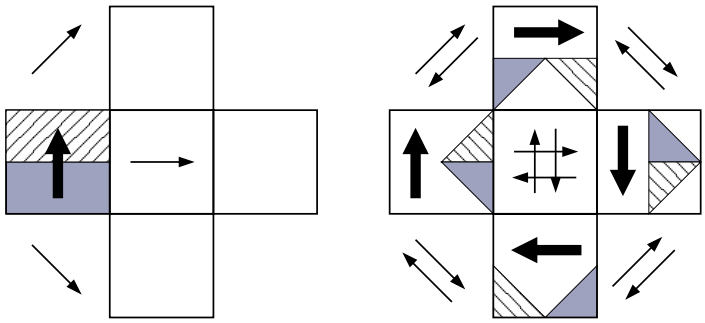

Figure 2. The figure illustrates the application of the two integration schemes discussed in the text for a set of $N_{\mathrm{s}}^{\mathrm{m}} = 4$ symmetry related tiles. Left panel: Selecting a generating tile at $\mathbf{K}_n$ allows its integration region to be restricted to $1/h_{\mathbf{K}_n}$ of its volume (shaded area). The integration over the full volume is recovered by application or equation (17) (represented by a thick arrow). The integrals for the other three tiles centred at $\mathbf{K}'_n$ are then obtained via equation (15) (indicated by thin arrows). Right panel: Restricting the integration in each tile to $1/h_{\mathcal{G}}$ of its volume. Application of equation (17) gives only $1/N_{\mathrm{s}}^{\mathrm{m}}$ of their proper values. The full integration region is recovered only by $(\mathrm{n}_{U'} - 1)$ applications of equation (15). In addition, note that the reduced volumes of the individual tiles have to be chosen in a consistent way.

Application of any operation U' with $U' \in \mathcal{G} \setminus \mathcal{G}_{\mathbf{K}_n}$ to a $\mathbf{k}$-point $\mathbf{k} \in V_{\mathbf{K}_n}$ leads by definition to a point $\mathbf{k}' \notin V_{\mathbf{K}_n}$. U' can therefore be used to generate a symmetry related tile starting from the $\mathbf{K}_n$-centred one. As we have to cover the whole Brillouin zone and as each tile of a set has the same symmetry as the selected representing or generating one there are exactly $h_{\mathcal{G}}/h_{\mathbf{K}_n}$ symmetry operations $U' \in \mathcal{G}$ to be considered. This is at the same time equal to the number of members $N_{\mathrm{s}}^{\mathrm{m}}$ of a set s introduced above.

The resulting scheme is illustrated in figure 2. Regrouping of the tiles leads to a set of four symmetry related tiles. Selecting the left tile to be the generating one the corresponding $\hat{\underline{\tau}}(\mathbf{K}_n)$ is evaluated first. This is done by performing the integration only over the irreducible volume $V_{\mathbf{K}_n}/h_{\mathbf{K}_n}$ (dark shaded). The integral over the full volume of the tile $V_{\mathbf{K}_n}$ is obtained by use of equation (17). Finally, the symmetry related scattering path operators $\hat{\underline{\tau}}(\mathbf{K}'_n)$ are obtained by equation (15). Altogether, using the procedure described above one has to perform an integration in $\mathbf{k}$-space over exactly the same volume as in the case of the CPA where no subdivision or tiling of the Brillouin zone is necessary.

Clearly, the scheme introduced here is not the only possible one. In fact one could also treat each tile separately and perform the integration only over a reduced volume $V_{\mathbf{K}_n}/h_{\mathcal{G}}$ that is in general smaller than that used above. Applying now equation (17) however covers only $h_{\mathbf{K}_n}/h_{\mathcal{G}}$ of the volume $V_{\mathbf{K}_n}$. Therefore, accounting for the rest of $V_{\mathbf{K}_n}$ can be achieved only by application of equation (15), i.e. by mapping the corresponding results from the other $(N_{\mathrm{s}}^{\mathrm{m}} - 1)$ members of the set to the tile at hand. To do this consistently their irreducible volume has to be chosen properly such as not to have integration regions covered twice while others are not accounted for. This alternative scheme once more demonstrates that within the NLCPA it is in fact possible to restrict the integration to $1/h_{\mathcal{G}}$ of the first Brillouin zone as in the standard CPA. This means also that for both schemes sketched in figure 2 an integration volume of the same size has to be

covered but its distribution over the Brillouin zone differs. However, it is obvious that the scheme described first is much easier to implement and leads to a minimum of overhead—in particular the number of applications of equations (15) and (17) is at its minimum as can easily be seen in figure 2. Therefore it is the most efficient one.

For the symmetry considerations above a non-relativistic formulation or a relativistic one applied to a non-magnetic system was assumed. When dealing with a magnetic system in a relativistic way these considerations have to be adapted. First of all one has to note that using a relativistic description for a magnetic system leads to a reduction in the number of symmetry operations as compared to the paramagnetic state that in addition depends on the orientation of the magnetization [30]. This of course does not affect the translational symmetry of a ferromagnetic solid and for that reason the construction of the clusters [18] is not affected. On the other hand, the reduction of the number of symmetry operations leads to an increase of the number of generating tiles in **k**-space. Assuming the magnetization along the z-direction—the geometry with the highest possible symmetry—one has for a face-centred cubic (fcc)-system with a cluster size of $N_c = 4$ a reduction from four to three generating tiles instead of two for the case of a non-magnetic system and/or a non-relativistic treatment. For a bcc-system with $N_c = 16$ the reduction is from 16 to seven instead of 16 to five, respectively. Also, the irreducible volume of the generating tiles is increased because of the lower symmetry. For the tile centred at the Γ-point, for example, the number of **k**-points to be dealt with is reduced only by a factor of 16 instead of 48 for the case of a non-magnetic system and/or a non-relativistic treatment. Finally one has to note that in the latter case only unitary symmetry operations U (see equation (15)) occur, while for the magnetically ordered case also anti-unitary symmetry operations that involve the time reversal operation may occur [30]. In spite of the various complications arising when dealing with magnetic systems, use of the above symmetry considerations leads to a substantial speed up of the calculations.

3. Application to FePt

We have implemented the NLCPA schemes outlined above within a program package that works for magnetic systems within a non- as well as a fully-relativistic framework [31]. The potentials used as input for the application of our NLCPA scheme presented below have been determined self-consistently by using the spin-polarized relativistic version of the KKR-CPA [27] within the framework of spin-density functional theory [32]. To demonstrate the application of the NLCPA we have chosen the alloy system fcc-$Fe_{0.5}Pt_{0.5}$ as it contains rather different alloy partners. While Fe has a high exchange splitting, leading in compounds and alloys to a spin-moment of 2–3μ_B, its spin–orbit splitting is relatively small. Pt, on the other hand, is non-magnetic as a pure metal and has a rather large spin–orbit splitting. Performing fully relativistic calculations for $Fe_{0.5}Pt_{0.5}$ that treat magnetic ordering and all relativistic effects on the same footing implies in particular that the corresponding single-site t-matrices $\underline{t}_\alpha (\alpha = \mathrm{Fe,Pt})$ are not diagonal. For these reasons applying the standard CPA to systems like $Fe_{0.5}Pt_{0.5}$ requires already the use of robust and efficient iteration algorithms as, for instance, the above mentioned Mills-algorithm [4]. Use of its counterpart described in section 2.2 together with the averaging and symmetrizing procedures allowed to perform NLCPA calculations for cluster sizes of up to four sites with only moderately more numerical effort than a standard CPA calculation. In particular, exploiting symmetry as described in section 2.3 led to a reduction in run time by about one order of magnitude in comparison to the unsymmetrized case.

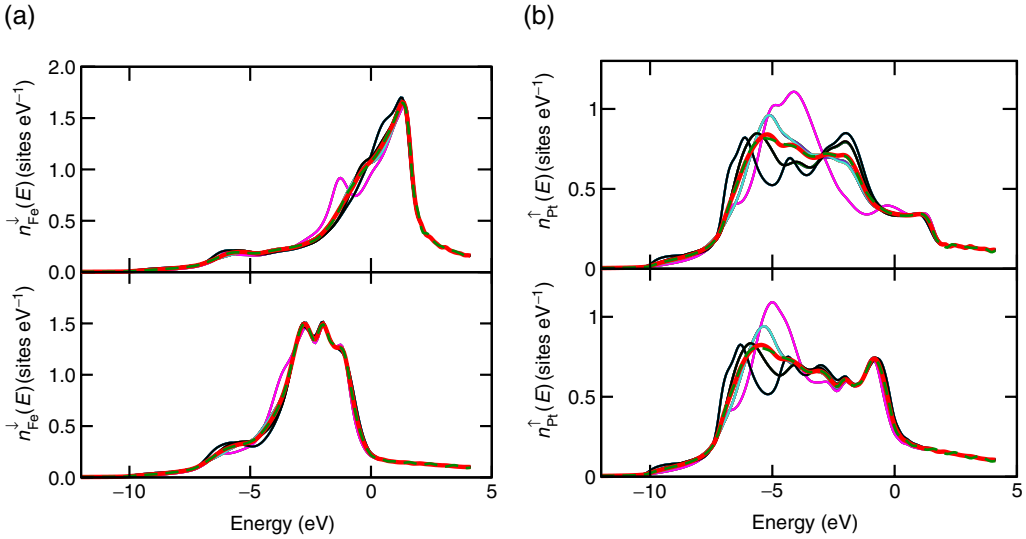

Figure 3. Spin-resolved DOS curves for Fe (top panel) and Pt (bottom panel) in $Fe_{0.5}Pt_{0.5}$ as obtained by the NLCPA. The thin lines represent the DOS for individual sites for all occurring cluster configurations for $N_c = 4$. The average NLCPA result is represented by a thick line, while the thick dashed line shows the CPA result, that for this system almost coincides with the NLCPA result. Note that a lot of the individual underlying cluster configurations are equivalent for symmetry reasons.

Figure 3 shows the resulting partial DOS for Fe and Pt in $Fe_{0.5}Pt_{0.5}$ obtained for a cluster with $N_c = 4$ sites. Here we assumed the magnetization to point along the z-direction. In dramatic departure from the conventional KKR-CPA calculations where only single-site partial DOS would be apparent, here the thin lines represent the DOS for all the $2^4 = 16$ different configurations. There is a rather strong variation within these sets of curves—in particular for Pt. Clearly, the average NLCPA result is however rather close to that obtained using the standard single-site CPA. Indeed, the average result would only differ significantly if short-range order was included.

In figure 4 the spin-magnetic moments for Fe and Pt are shown as a function of the cluster occupancy together with the NLCPA result. For Fe one notes only a fairly weak fluctuation around the NLCPA average. This is because the spin moment in this fcc system is already around $3\mu_B$, i.e. it is essentially saturated. Nevertheless, one notes a clear increase of the Fe moments with decreasing Fe content in the cluster. This is fully in line with the concentration dependence of the Fe moment in the alloy: with decreasing Fe concentration the spin magnetic moment in fcc-Fe_xPt_{1-x} increases [33]. Another interesting finding is that clusters that are inequivalent due to the inclusion of spin–orbit coupling nevertheless have essentially the same spin-magnetic moment. Using for $N_c = 4$ the cluster geometry as suggested by Rowlands *et al* [15, 16], the cluster sites correspond to the corners of a tetrahedron with two sites lying in the basal plane of a cube at $z = 0$ and two at $z = 1/2$. For the spin-moment it obviously does not matter much whether for example for a cluster of two Fe atoms and two Pt atoms the Fe atoms are both in the basal plane or one is at $z = 0$ and the other at $z = 1/2$ (in contrast to a non-relativistic calculation these two situations are inequivalent as we account for spin–orbit coupling and assume the average magnetization to point along the z-direction). As opposed to Fe, the induced spin magnetic

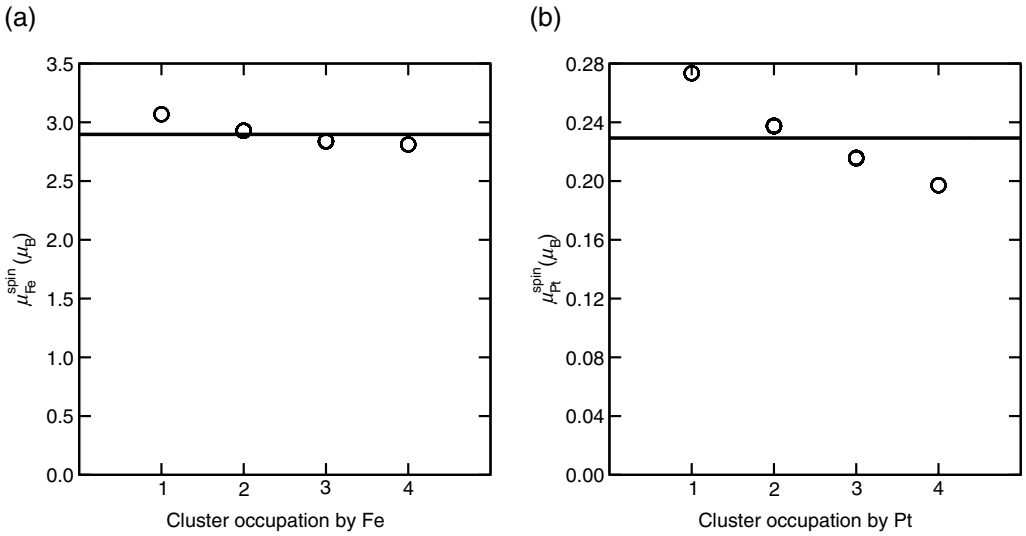

Figure 4. Spin magnetic moment of Fe and Pt as obtained by the NLCPA. The various data points show the moments for individual sites of all occurring cluster configurations for $N_c = 4$ as a function of the occupation of the cluster by Fe and Pt atoms, respectively. The horizontal lines represent the average NLCPA result, that nearly coincides with the CPA result.

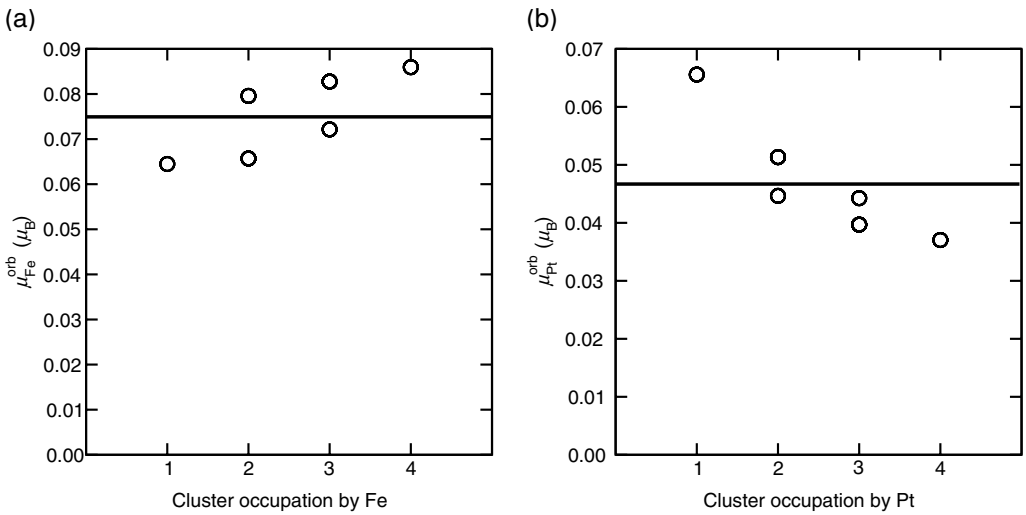

Figure 5. As for figure 4 but for the orbital moments of Fe and Pt.

moment of Pt depends much more on the specific cluster configuration. Again in line with the average Pt moment obtained as a function of the concentration in disordered fcc-Fe_xPt_{1-x} the Pt moment increases when the Pt content within a cluster is reduced. This behaviour confirms the expectation that an increase of the number of magnetic Fe atoms as nearest neighbours should induce a higher spin magnetic moment on Pt. As for the spin moment of Fe, there is hardly any dependence on the geometry of a cluster for a given occupation number.

The results for the spin–orbit induced orbital magnetic moments are shown in figure 5. As one notes, for Fe the scatter of these moments is noticeably larger than for the spin magnetic moment.

One reason for this is that there is no restriction present due to saturation. The other reason is that orbital magnetic moments induced by spin–orbit coupling are quite sensitive to the DOS at the Fermi level that here shows pronounced scatter (see figure 3). This can be demonstrated by application of perturbation theory that allows to express the spin–orbit induced moment in terms of the spin–orbit coupling strength and the spin- and orbital resolved DOS at the Fermi level [34]. In line with this we do not only find a pronounced variation of $\mu_{\mathrm{Fe}}^{\mathrm{orb}}$ with the occupation number of the cluster but also on the cluster configuration for a given occupation number. For example the moments for a cluster with two Fe atoms at $z = 0$ differ from a cluster with a Fe atom at $z = 0$ and $z = 1/2$. If all cluster configurations were given the same weight P_γ (see equation (5)) there would of course be no change in the magntitude of the orbital moment when the magnetization is oriented, e.g. along the x-direction instead of pointing along the z-direction. On the other hand, assuming a short range order that would make these two situations inequivalent this would lead to an anisotropy in the orbital magnetic moment. For the spin–orbit induced orbital moment of Pt we find a similar behaviour as for Fe. Because of the larger spin–orbit coupling strength $\mu_{\mathrm{Pt}}^{\mathrm{orb}}$ is nearly as high as $\mu_{\mathrm{Fe}}^{\mathrm{orb}}$ although $\mu_{\mathrm{Pt}}^{\mathrm{spin}}$ is much smaller than $\mu_{\mathrm{Fe}}^{\mathrm{spin}}$.

Finally one should note that similar investigations on the environmental influence on magnetic properties have also been done in the past on the basis of the ECM [35] and using supercell techniques [36]. However, as a self-consistent theory, the NLCPA obviously supplies a much more sound and efficient basis for this type of investigation, particularly in the presence of short-range order.

4. Summary

In this paper we have proposed a fully relativistic formulation of the KKR-NLCPA which is designed for the treatment of magnetically-ordered alloys. Crucial to its implementation is a reformulation of the algorithm by the adaption of the so-called Mills-CPA-algorithm, leading to a very robust and efficient iteration scheme. An additional and substantial reduction of numerical effort could be achieved by making use of symmetry. As a consequence the computational effort for the Brillouin zone integration in the NLCPA is essentially the same as in the CPA. We note that there is of course increased computational cost in real space due to averaging over the 2^{N_c} cluster configurations (where N_c is the number of sites in the cluster), and importance sampling of the configurations is needed for large cluster sizes. We also note that the methods introduced in this paper equally apply to the non-relativistic case and thus can also be used to achieve an efficient and robust implementation of the non-relativistic KKR-NLCPA technique.

The power of the scheme presented here was demonstrated by an application to the random alloy system fcc-$Fe_{0.5}Pt_{0.5}$. The most remarkable result for this system is that within clusters of given composition but different configuration there is hardly any difference of the spin magnetic moment (in the absence of short-range order). For the spin–orbit induced orbital moments, on the other hand, a pronounced variation for the different configurations is present.

In contrast to the standard CPA, the NLCPA allows us to study not only the configurational average but also the influence of cluster configurations contributing to the average. This has been demonstrated here by the results for the FePt system, and further possible investigations include applying a non-random cluster probability distribution to study the influence of short-range order. Therefore the NLCPA supplies a formal basis for a discussion of inhomogeneous line broadening as seen for example in core level photo emission [37] and Mössbauer-spectroscopy [35] of

disordered systems. The NLCPA could also have an important impact in magneto-resistance calculations, for example the study of the influence of short-range order on magnetic anisotropy.

Acknowledgment

This work was supported by the Deutsche Forschungsgemeinschaft within the priority program 'Moderne und universelle first-principles-Methoden für Mehrelektronensysteme in Chemie und Physik' (SPP 1145/2).

References

[1] Soven P 1967 *Phys. Rev.* **156** 809
[2] Stocks G M, Temmerman W M and Györffy B L 1978 *Phys. Rev. Lett.* **41** 339
[3] Winter H and Stocks G M 1983 *Phys. Rev.* B **27** 882
[4] Ebert H and Akai H 1993 *Int. J. Mod. Phys.* B **7** 922
[5] Winter H, Durham P J and Stocks G M 1984 *J. Phys. F: Met. Phys.* **14** 1047
[6] Butler W H 1985 *Phys. Rev.* B **31** 3260
[7] Tsukada M 1972 *J. Phys. Soc. Japan* **32** 1475
[8] Mills R, Gray L J and Kaplan T 1983 *Phys. Rev.* B **27** 3252
[9] Mookerjee A 1987 *J. Phys. F: Met. Phys.* **17** 1511
[10] Gonis A, Stocks G M, Butler W H and Winter H 1984 *Phys. Rev.* B **29** 555
[11] Gonis A 1992 *Green functions for ordered and disordered systems* (Amsterdam: North-Holland)
[12] Rowlands D A 2006 *J. Phys. Condens. Matter* **18** 3179
[13] Jarrell M and Krishnamurthy H R 2001 *Phys. Rev.* B **63** 125102
[14] Hettler M H, Tahvildar-Zadeh A N, Jarrell M, Pruschke T and Krishnamurthy H R 1998 *Phys. Rev.* B **58** R7475
[15] Rowlands D A 2004 *PhD Thesis* University of Warwick
[16] Rowlands D A, Staunton J B and Györffy B L 2003 *Phys. Rev.* B **67** 115109
[17] Rowlands D A, Staunton J B, Györffy B L, Bruno E and Ginatempo B 2005 *Preprint* cond-mat/0411347
[18] Rowlands D A, Staunton J B, Györffy B L, Bruno E and Ginatempo B 2005 *Phys. Rev.* B **72** 045101
[19] Biava D A, Ghosh S, Johnson D D, Shelton W A and Smirnov A V 2005 *Phys. Rev.* B **72** 113105
[20] Rowlands D A, Ernst A, Györffy B and Staunton J B 2006 *Phys. Rev.* B **73** 165122
[21] Abrikosov I A, Niklasson A M N, Simak S I, Johansson B, Ruban A V and Skriver H L 1996 *Phys. Rev. Lett.* **76** 4203
[22] Nicholson D M C, Stocks G M, Wang Y, Shelton W A, Szotek Z and Temmerman W M 1994 *Phys. Rev.* B **50** 14686
[23] Stocks G M, Nicholson D M C, Wang Y, Shelton W A, Szotek Z and Temmerman W M 1994 *Proc. 1994 Simul. Multiconf.* ed A M Tentner (San Diego: The Society of Computer Simulations)
[24] Ujfalussy B, Faulkner J S, Moghadam N Y, Stocks G M and Wang Y 2000 *Phys. Rev.* B **61** 12005
[25] Ginatempo B and Staunton J B 1988 *J. Phys. F: Met. Phys.* **18** 1827
[26] Rose M E 1961 *Relativistic Electron Theory* (New York: Wiley)
[27] Ebert H 2000 *Electronic Structure and Physical Properties of Solids (Lecture Notes in Physics vol 535)* ed H Dreyssé (Berlin: Springer) p 191
[28] Huhne T and Ebert H 2002 *Phys. Rev.* B **65** 205125
[29] Bradley C J and Cracknell A P 1972 *The Mathematical Theory of Symmetry in Solids* (Oxford: Clarendon)
[30] Cracknell A P 1969 *J. Phys. C: Solid State Phys.* **2** 1425
[31] Ebert H *et al* 2002 *The Munich SPR-KKR package*, version 2.1.1. Online at http://olymp.cup.uni-muenchen.de/ak/ebert/SPRKKR
[32] Vosko S H, Wilk L and Nusair M 1980 *Can. J. Phys.* **58** 1200

[33] Paudyal D, Saha-Dasgupta T and Mookerjee A 2004 *J. Phys.: Condens. Matter* **16** 2317
[34] Popescu V, Ebert H, Nonas B and Dederichs P H 2001 *Phys. Rev.* B **64** 184407
[35] Ebert H, Winter H, Györffy B L, Johnson D D and Pinski F J 1987 *Solid State Commun.* **64** 1011
[36] James P, Eriksson O, Johansson B and Abrikosov I A 1999 *Phys. Rev.* B **59** 419
[37] Cole R J, Brooks N J and Weightman P 1997 *Phys. Rev. Lett.* **78** 3777